

Calculation of Surface Speciation on Mild Steel under Applied Polarization

Zheng Ma, Bruce Brown, Srdjan Netic, and Marc Singer
Institute for Corrosion and Multiphase Technology (ICMT), Ohio University
342 West State Street
Athens, OH, 45701
USA

ABSTRACT

The rates of electrochemical and precipitation reactions taking place on the steel surface are dependent on the chemistry of the aqueous phase in contact with the substrate. While the bulk speciation is often used to characterize the severity of the environment, large differences can exist between bulk and surface chemistries, leading to inaccurate representation of the corrosion phenomena. This issue requires a better understanding of the surface speciation. Given the fact that directly measuring surface speciation is a very challenging task, corrosion models must be employed to calculate these surface parameters based on the bulk chemistry. In the present work, an electrochemical model was developed for that exact purpose and used to predict corrosion behavior not only at the corrosion potential, but also under applied polarization, where surface and bulk chemistries differ greatly. This model has been extensively calibrated against experimental results in both corrosion product free conditions as well as in conditions where corrosion product layers form.

Keywords: carbon steel, corrosion rate, modeling, uniform corrosion, carbon dioxide, hydrogen sulfide

INTRODUCTION

It has been well understood that corrosion product layers can precipitate on the surface of mild steel in both sweet corrosion (CO_2 dominated) and sour corrosion (H_2S dominated) environments. However, all the current kinetics models focused on corrosion product layer formation are proposed based on bulk speciation¹⁻⁵. This situation is understandable: most of kinetics related parameters used in these models can either be measured directly from the bulk solution, or can be estimated through a simple bulk water chemistry model; not to mention the fact that the predictions from some of the bulk speciation-based kinetics models have been proven accurate within an acceptable range.

To separate the effects from “precipitation” and “corrosion”, the two processes that normally occur simultaneously during corrosion product formation, a cathodically protected iron substrate and an actively corroding iron substrate were used for corrosion product layer precipitation in the authors

previous study⁴⁻⁶. For experiments using the cathodically protected substrate, a cathodic polarization (-50~-100 mV vs. OCP) was applied to ensure that substrate corrosion was minimized and the precipitation of corrosion product layer was the dominant process during measurement; for experiments using the actively corroding substrate, both the precipitation and spontaneous iron corrosion were taking place at the substrate surface. Figure 1 compares predictions and measured data at 50°C (the lowest experiment temperature) on the left and 80°C (the highest experiment temperature) on the right. The results from two different substrates do not completely overlap with each other, yet they are similar in magnitude, and most of the results from the actively corroding surface are lower than the results from the cathodically protected surface within a factor of two. This means the surface speciation did not affect FeCO₃ precipitation kinetics significantly, at least in these tested conditions.

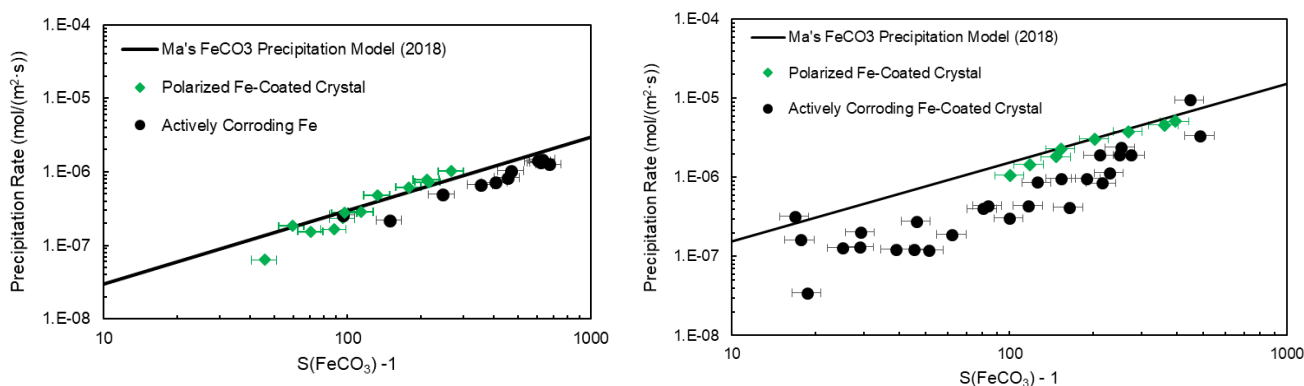


Figure 1. Comparison between model predictions and experimental results for FeCO₃ precipitation rate on different substrates at 50°C (left) and 80°C (right), 1 wt% NaCl, 1 bar total pressure.

Different phenomena, however, have been observed when a similar study was performed for mackinawite precipitation kinetics in a solution with a much lower FeS saturation value. Part of the experimental results are shown in Figure 2. It can be seen from the experimental results obtained at 80°C, that the precipitation rate, PR_{FeS} , measured on an actively corroding substrate was slightly lower than on a cathodically protected specimen by a factor of two when the S_{FeS} was higher than 10, similar to what had been observed in FeCO₃ precipitation measurements. However, the discrepancy between the PR_{FeS} of these two surfaces became larger with the decrease of the bulk S_{FeS} value. It was also noticed that the PR_{FeS} was less dependent on S_{FeS} when using the cathodically protected specimen, *i.e.*, the PR_{FeS} was only reduced by 3-4 times when the measured S_{FeS} was changed by about three orders of magnitude. In addition to that, according to recorded PR_{FeS} , FeS was continuously precipitating on the electrically polarized surface even when the bulk $S_{FeS} < 1$. The results for cathodically protected specimen were examined at different temperatures and it was found that the FeS precipitation continued even when the solution was highly under saturated in all tested cases, as illustrated in Figure 2 (right).

Based on these observations, it can be concluded that the speciation difference between bulk conditions and surface conditions might be small enough to be ignored for CO₂ corrosion, as in the cases for FeCO₃ precipitation. However, the examples of FeS precipitation point out that the speciation difference could be significantly large in sour conditions, and bulk speciation calculations may no longer accurately describe the speciation on the substrate surface, where the precipitation takes place. This requires a better understanding of the surface speciation, especially for those obtained from the

electrically polarized substrates. Given the fact that “directly” measuring surface speciation is an impossible task, corrosion models must be employed to estimate these parameters. Three currently available in-house corrosion models will be briefly discussed.

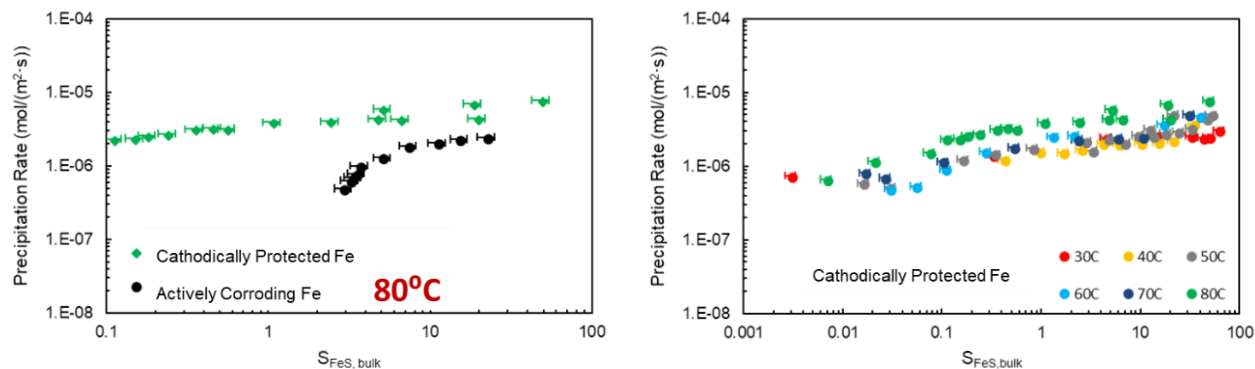


Figure 2. Comparison of experimental results for FeS precipitation kinetics. 1 wt% NaCl, 1 bar total pressure. Left: PR_{FeS} on different substrates at 80°C; right, PR_{FeS} on cathodically protected specimens at different temperatures.

FREECORP 1.0 is a steady-state electrochemical corrosion prediction model, strongly rooted in theory, and all the parameters in which are calculated based on the bulk solution parameters. This model will be referred to as a “*steady-state*” model. All the related chemical reactions are assumed to be in equilibrium, so that the kinetics of chemical reactions can be ignored. The formation of $FeCO_3$ and FeS in the *steady-state* model is calculated using empirical correlations in order to improve the accuracy of corrosion rate prediction. This model is simple and easy to be understood. It can provide reasonable predictions for many different conditions ⁷. However, due to the lack of surface speciation information in the *steady-state* model, this model cannot be used to interpret the FeS results as showed previously.

MULTICORP™, on the other hand, is and will be referred to as a “*fully mechanistic*” corrosion prediction model. Almost all the missing pieces from the *steady-state* model have been accounted for in the *fully mechanistic* model. This model discretizes the domain from the bulk solution to the metal surface into hundreds of small control volumes, called nodes, and calculates all the interactions of the species at each node throughout the liquid boundary layer. This model solves 2nd order non-linear partial differential equations, which were derived from fundamental physico-chemical relationships, for each single node. Accurate predictions for speciation on the steel surface can be obtained from this *fully mechanistic* model; however, the model is more complicated and requires more computing power.

Zheng’s *Two Nodes Model* ⁸ has more detailed computations than the *steady-state* model, but is not as complicated as the *fully mechanistic* model. This model has one node at the bulk solution interface and another node on the steel surface. The fundamental physico-chemical laws are applied to both nodes, which is similar to the *fully mechanistic* model. However, this model eliminates the process calculations in the boundary layer between the two nodes, which is similar to the *steady-state* model, and assumes the concentration gradient within the boundary layer to be linear. Another simplification that has been made for this model is that all the chemical reactions are assumed to be in equilibrium on the steel surface except for CO_2 hydration. Prior to this research, neither the *fully mechanistic* model nor the *Two Nodes Model* could calculate conditions at an electrically polarized metal surface in solution, a condition that needed to be addressed in order to explain the FeS precipitation results as shown in Figure 2. To

solve this, the *Two Nodes Model* was modified to calculate surface speciation at a cathodically protected metal surface because this model has a good balance of accuracy and simplicity.

DESCRIPTION OF SURFACE SPECIATION CALCULATION WITH APPLIED POLARIZATION

The *Two Nodes Model* used in this research has three main parts to describe H₂S/CO₂ corrosion⁸:

1. A water chemistry model to calculate speciation in the bulk solution.
2. An electrochemical corrosion model including the process of mass transfer from bulk to surface to calculate surface speciation and corrosion rate under an applied potential. The effect of corrosion product layer precipitation on surface speciation was not considered.
3. A corrosion product precipitation and growth model for both FeCO₃ and FeS. Parameters related to surface speciation and corrosion rate under applied potential were calculated in a condition of corrosion product layer precipitation.

The methodology of calculating bulk speciation has been addressed in the literature related to both CO₂⁹ and H₂S corrosion¹⁰ and will not be repeated here. The principles of the latter two models will be briefly covered in this section since modifications have been made to enable the surface speciation calculation under applied polarization. This modified version of the *Two Nodes Model* will be referred to as the *Polarization Model*.

Electrochemical Corrosion Model

The *Two Nodes Model* considers one node on the steel surface and another node in the bulk solution as shown in Figure 3. The calculation of species concentration starts with a mass conservation on the steel surface:

$$\frac{\partial c_{surface,j}}{\partial t} = \frac{N_{in,j} - N_{out,j}}{\Delta x} + R_j \quad (1)$$

where $N_{in,j} - N_{out,j}$ calculates the net flux caused by mass transfer from bulk to surface as well as heterogeneous electrochemical reactions; R_j is the production of homogeneous chemical reactions, and Δx represents the thickness of the boundary layer between the steel surface and bulk solution. In this model, the species concentration in the bulk solution, $c_{bulk,j}$, is calculated using the *steady-state* model's bulk water chemistry calculations.

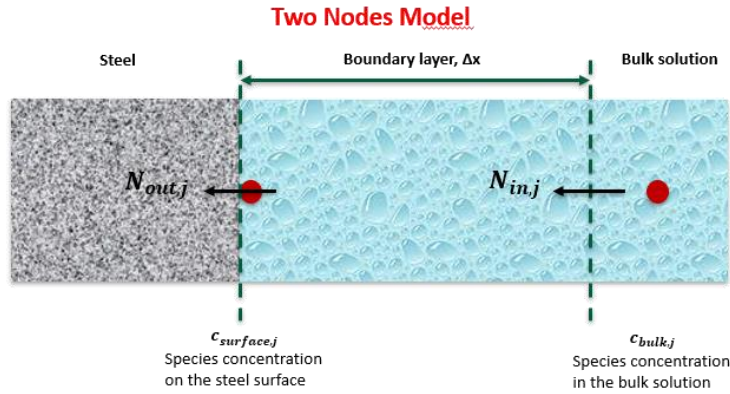


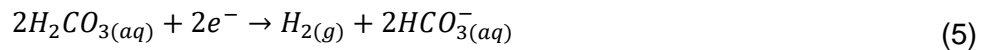
Figure 3. Illustration for the mass transport governing equation and computation domain of the Two Nodes Model.

To calculate the flux of mass transfer, the diffusion due to concentration gradient (considered for all species) and the electromigration due to potential gradient (only considered for Na^+ and Cl^- because of their much higher concentrations as compared to the rest) are both included:

$$N_{in,j} = \underbrace{k_{m,j}(c_{bulk,j} - c_{surface,j})}_{\text{Diffusion due to concentration gradient}} + \underbrace{k_{m,j} \frac{z_j F}{RT} c_{bulk,j} \Delta \Phi}_{\text{Electromigration due to potential gradient}} \quad (2)$$

Where $k_{m,j}$ is mass transfer coefficient; $c_{bulk,j}$ and $c_{surface,j}$ are species concentration in bulk solution and on steel surface respectively; z_j is the electric valency of the calculated species; $\Delta \Phi$ is electrical potential difference between the two nodes; F , R , and T are Faraday's constant, gas constant, and temperature, respectively.

Several heterogeneous electrochemical reaction terms are considered in this model, which include iron dissolution (Reaction (3)), proton reduction (Reaction (4)), H_2CO_3 reduction (Reaction (5)), H_2S reduction (Reaction (6)), and water reduction (Reaction (7)).



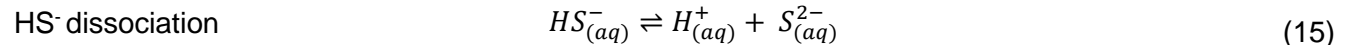
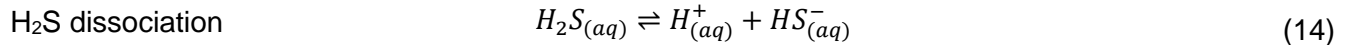
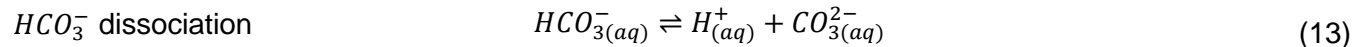
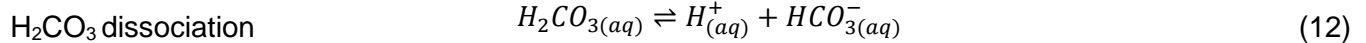
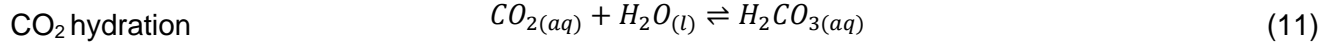
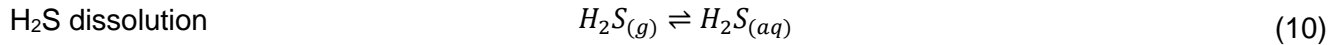
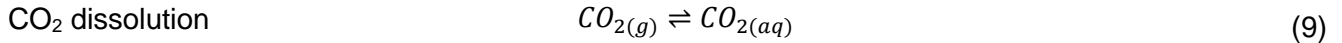
For each reaction, the flux at steel surface can be calculated through Equation (8):

$$N_{out,j} = \pm \frac{i_j}{n_j F} \quad (8)$$

Where i_j is current density for a given species, and n_j is the number of exchanged electrons per mol of the given species in the electrochemical reactions.

One should note that the direct electrochemical reductions of H_2CO_3 and H_2S are used in this model. According to current literature, the mechanisms for both CO_2 ^{11, 12} and H_2S ¹³ corrosion of mild steel are caused by their dissociation reactions and buffering effect to provide $[H^+]$ instead of directly reducing at the metal surface. However, it can be argued that the difference in calculated corrosion rates between the two possible mechanisms for CO_2 corrosion are minor until reaching a relatively high CO_2 partial pressure (at least 10 bar pCO_2)¹¹. Consequently, predictions based on the direct reduction of H_2CO_3 mechanism should be quantitatively correct under the tested conditions. It is also reasonable to assume that this argument holds true for the case of H_2S corrosion. Models based on these two different mechanisms have been shown to produce good agreement with corrosion rate results over their respective temperature and pressure ranges^{2, 13}.

The term $(\Delta x * R_j)$ is related to homogeneous chemical reactions, where CO_2 and H_2S dissolutions, CO_2 hydration, and H_2CO_3 and H_2S dissociations are included for Equation (1):



After these calculations, Equation (16) can be obtained for each participating species by substituting the flux of mass transfer, electrochemical reactions, and chemical reactions into the mass balance equation of Equation (1):

$$\Delta x \frac{\partial c_{surface,j}}{\partial t} = \pm \frac{i_j}{n_j F} + k_{m,j}(c_{bulk,j} - c_{surface,j}) + k_{m,j} \frac{z_j F}{RT} c_{bulk,j} \Delta \Phi + \Delta x * R_j \quad (16)$$

In addition to Equation (8) for each species, the electro-neutrality equation is always valid on the steel surface:

$$\sum z_j c_{surface,j} = 0 \quad (17)$$

Instead of calculating surface speciation only at the corrosion potential by using the charge balance equation, Equation (18), the applied potential is required as an input to solve surface speciation when using under polarization conditions. To do so, substitute E in Equation (19) with the working potential. Detailed information about reference current density i_0 , reference potential E_0 , and Tafel slope b for reactions (3) - (7) can be found from literature².

$$\sum i_a = \sum i_c \quad (18)$$

$$i_j = i_0 \times 10^{\pm \frac{E-E_0}{b}} \quad (19)$$

Therefore, chemical component speciation on a polarized specimen surface can be calculated through Equation (16) - (19) using this methodology.

Corrosion Product Layer Growth Model

The layer growth model proposed by Lee and Nestic in 2003¹⁴ was employed if a corrosion product layer is formed in system:

$$\frac{\partial \varepsilon}{\partial t} = - \frac{M_{FeCO_3/FeS}}{\rho_{FeCO_3/FeS}} \cdot PR_{FeCO_3/FeS} + CR \frac{1 - \varepsilon}{\Delta x} \quad (20)$$

According to this model, the change of porosity of the corrosion product layer, $\frac{\partial \varepsilon}{\partial t}$, is a balance between the precipitation of a corrosion product layer, represented by the term $\left(\frac{M_{FeCO_3/FeS}}{\rho_{FeCO_3/FeS}} \cdot PR_{FeCO_3/FeS} \right)$, and the undermining effect due to iron dissolution, represented by the term $\left(CR \frac{1-\varepsilon}{\Delta x} \right)$ where CR is short for corrosion rate.

The appearance of a corrosion product layer affects the system in two ways. It can reduce the rate of electrochemical reactions by blocking the reaction sites if the formed layer is well attached on steel surface and it can act as a diffusion barrier to slow down the species transportation between bulk solution and steel surface. These two effects are addressed by Equation (21) and Equation (22):

$$i = \pm \varepsilon \times i_0 \times 10^{\pm \frac{E-E_0}{b}} \quad (21)$$

$$k_{s,j} = \frac{\varepsilon \tau D_j}{\delta} \quad (22)$$

Where $k_{s,j}$ is mass transfer coefficient; τ is tortuosity; D_j is diffusion coefficient through the corrosion product layer; δ is the thickness of the layer and it is also a function of precipitation rate³.

By taking the effects of layer formation into consideration, the mass conservation equation as shown in Equation (16) needs to be rewritten:

$$\Delta x \frac{\partial c_{surface,j}}{\partial t} = \pm \varepsilon \frac{i_j}{n_j F} + k_{s,j}(c_{bulk,j} - c_{surface,j}) + k_{s,j} \frac{z_j F}{RT} c_{bulk,j} \Delta \Phi + \Delta x * R_j \quad (23)$$

From this equation, the blocking effect and the diffusion barrier effect are both considered, and the surface speciation can be calculated by solving Equation (23) and Equation (17) simultaneously for an electrically polarized metal surface when using a controlled working potential for the E term in Equation (21).

MODEL VERIFICATION

The *Polarization Model* needs to be extensively verified before it can be confidently used as a prediction tool for surface speciation calculation on a cathodically polarized steel surface. In this section, model predictions are compared with experimental results in both bare steel conditions and conditions where growth of corrosion product layer occurs. In the former case, model predictions are compared with experimentally measured polarization curves; in the latter case, model predictions are compared with corrosion rate and measured surface pH changes during the precipitation of FeCO_3 . Most of the lab results are taken from Zheng's dissertation data² unless otherwise stated.

Verification of Polarization Model in Bare Steel Conditions

Figure 4 compares the effect of solution pH on CO_2 corrosion mechanisms as observed by potentiodynamic sweep data. According to the lab data (shown as solid lines), when bulk solution pH was the only parameter changed, the limiting current density on cathodic polarization curve increased as a result of more protons available in a low pH solution. Model predictions (dashed lines) were able to capture this behavior. A good agreement between model prediction and experiment results were achieved at pH4. The predicted limiting current density was lower than the measured value at pH5 and the difference became larger at lower cathodic potentials. This difference could be caused by possible experimental errors or may be some adjustments are required to improve the model's accuracy. However, the discrepancy is less prominent when the potential is between 0.78V-0.82V vs. Sat. KCl, Ag/AgCl reference electrode as highlighted by the colored bar, a potential range that was commonly used for those previously mentioned precipitation kinetic measurements.

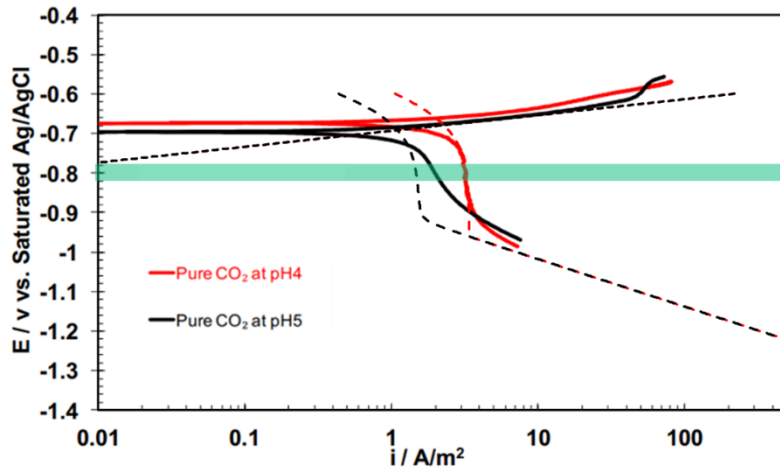


Figure 4. Comparison between the Polarization Model and experiments for CO₂ sparged environment, 30°C, RCE, 1000 rpm, P_{total} = 1 atm, 1wt% NaCl.

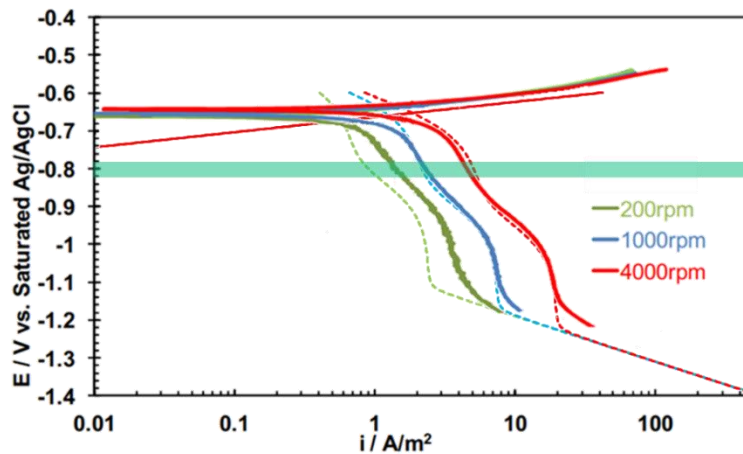


Figure 5. Comparison between the Polarization Model and experiments for H₂S sparged environment, 30°C, pH 4, 0.97 mbar p_{H₂S}, balance nitrogen, P_{total} = 1 atm, 1wt% NaCl.

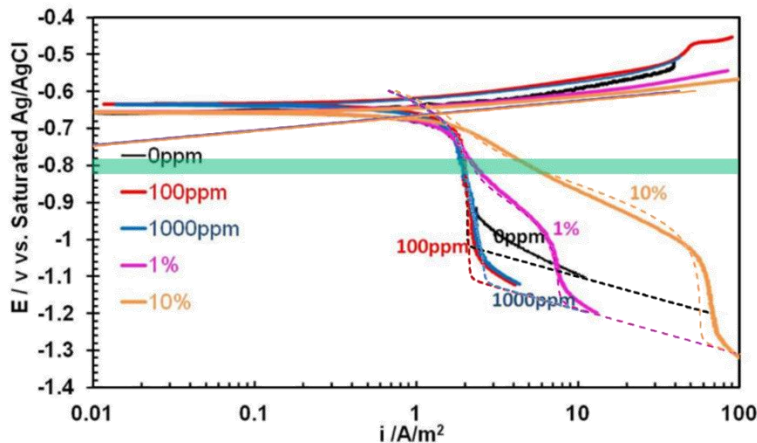


Figure 6. Comparison between model and experiments for H₂S sparged environment, 30°C, pH 4, RCE, 1000 rpm, varied ppm H₂S, balance nitrogen, P_{total} = 1 atm, 1wt% NaCl.

The effect of flow velocity on corrosion behavior in an H₂S environment is shown in Figure 5. Same as the last case, the solid lines are for measured results and the dashed lines are for model predictions. The double wave behavior that usually can be observed in H₂S environment² appears for each case. In addition to that, an increased mass transfer rate of species caused by the increased flow velocity accelerated the limiting current density. Model prediction successfully catches both the double wave behavior and the current density accelerating behavior. Except for the case with 200 rpm rotating speed, the model agrees well with experimental data.

Comparison was also performed in conditions with different H₂S concentrations. According to Zheng, the H₂O reduction reaction would be retarded due to the presence of H₂S, but this retardation effect was not dependent on the H₂S concentration¹⁵. This theory is supported by both experimental results and model predictions in Figure 6. In addition, the model was able to predict the double wave behavior introduced by H₂S reduction. The model also predicts the limiting current density change related to the change of H₂S concentration.

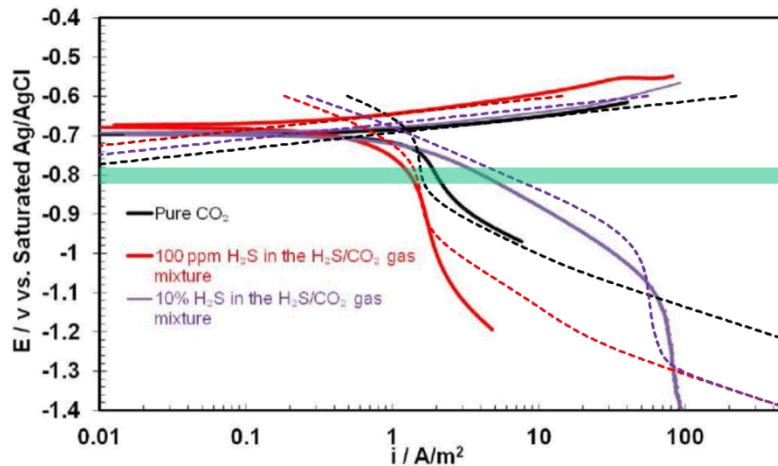


Figure 7. Comparison between the Polarization Model and experiments for H₂S/CO₂ environment, 30°C, pH 4, RCE, 1000 rpm, P_{total} = 1 atm, 1wt% NaCl.

Finally, model prediction is compared with laboratory data in H₂S/CO₂ mixture environment. Figure 7 shows the model captures the water retardation effect and the limiting current density accelerating effect. The predicted polarization curves generally agree with measured curves.

Verification of Polarization Model in Layer Formation Conditions

Comparisons between the current model predictions and experimental data for corrosion rate change during FeCO₃ precipitation are presented Figure 8 with different initial [Fe²⁺]. It should be noted that the initial corrosion rate (@ t=0) was independent of the initial [Fe²⁺] as it was measured prior to the formation of a corrosion product layer. However, the decrease of corrosion rate was faster when the initial [Fe²⁺] was higher. The reason for this is that the precipitation rate of FeCO₃ is linearly related to the saturation value of FeCO₃ where a higher [Fe²⁺] leads to a higher FeCO₃ saturation. As previously discussed for Equation (20)-(21), a faster precipitation rate would promote the decrease of corrosion product layer porosity and reduce the corrosion rate more significantly. Good agreement between model prediction and experimental data indicate the model is highly capable of simulating the FeCO₃ precipitation kinetics and also the effect of FeCO₃ precipitation on the corrosion behavior.

One of the main expected applications of the present model is to predict surface pH during the corrosion process. Not only because the specimen surface is the true location for both corrosion and precipitation to take place, but also because the surface pH measurement is tedious and cannot be measured as straightforward as bulk pH measurement even in lab testing, not to mention how difficult it could be to measure that value in the field of oil and gas production and transportation.

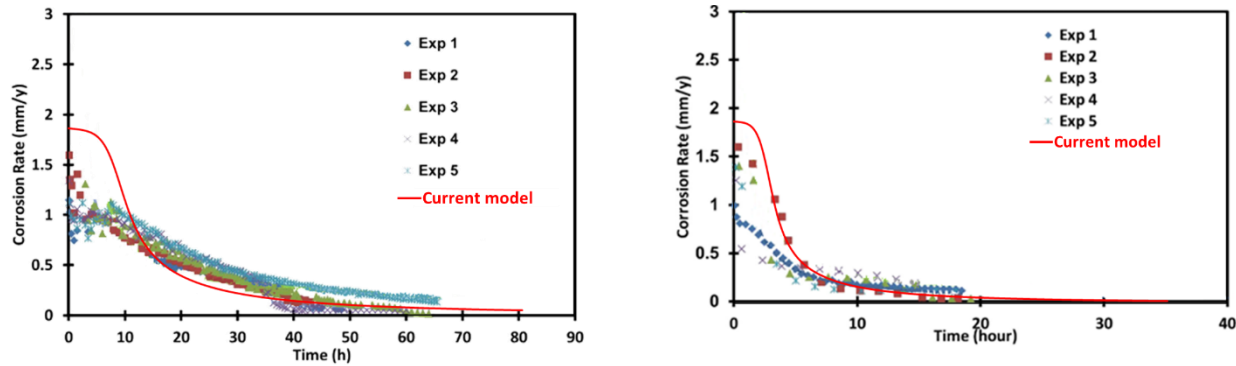


Figure 8. Comparison between model and experiments during FeCO_3 precipitation, 80°C , pH 6.6, RCE, 1000 rpm, $P_{\text{total}} = 1$ atm, 1wt% NaCl, initial $[\text{Fe}^{2+}] = 10$ ppm (left) and $[\text{Fe}^{2+}] = 50$ ppm (right).

A specially designed system using a flat surface pH probe¹⁶ to measure pH of a metal surface provides the next set of data¹⁷. The surface pH shown in Figure 9 was measured using a piece of mild steel wire-mesh flush-mounted against the tip of a flat pH probe. As the mild steel mesh corroded during the experiment, the pH directly behind the steel mesh surface would change as measured by the flat surface pH probe.

According to the measurement, bulk pH was stable throughout the 12 days test due to the strong buffering effect from H_2CO_3 . In addition, the measured surface pH was always higher than that in the bulk solution, as the system is in electro-neutrality ($c_{\text{Na}^+_{\text{surface}}} = c_{\text{Cl}^-_{\text{surface}}}$ is omitted in Equation (24)):

$$2c_{\text{Fe}^{2+}_{\text{surface}}} + c_{\text{H}^+_{\text{surface}}} = c_{\text{HCO}_3^-_{\text{surface}}} + 2c_{\text{CO}_3^{2-}_{\text{surface}}} + 2c_{\text{OH}^-_{\text{surface}}} \quad (24)$$

The $c_{\text{Fe}^{2+}_{\text{surface}}}$ on the left-hand side of equation increased due to the actively corroding specimen. Because the experiment was performed in an open system and purged constantly with CO_2 , the three terms on the right-hand side of the equation were all constant. Due of this, surface pH was higher since the $c_{\text{H}^+_{\text{surface}}}$ decreased during the process to keep electro-neutrality valid.

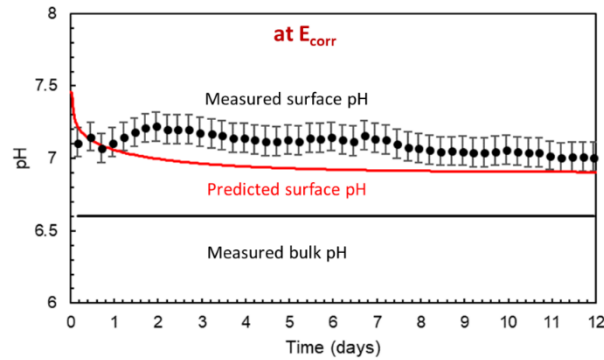


Figure 9. Comparison between the Polarization Model and experiments¹⁷ during FeCO_3 precipitation, 80°C , pH 6.6, $P_{\text{total}} = 1 \text{ atm}$, 1wt% NaCl.

When comparing the measured surface pH with model prediction, a close agreement is achieved. The difference is within 0.2 pH units. This proved the present model can provide a rather accurate surface pH prediction in layer formation conditions.

SURFACE SPECIATION PREDICTIONS

Since the current polarization model was proven to be accurate under multiple environmental conditions, it can now be used to evaluate the difference between bulk condition measurements and surface speciation calculations during the formation process of corrosion product layer in sweet and sour environments. Comparisons are made on both actively corroding specimens and cathodically polarized specimens. All the measured data are taken from the author's previous experiments.

In FeCO_3 Formation Environment

Surface speciation in FeCO_3 formation environment will be predicted using the present model. Two sets of parameters will be compared: the difference between the predicted surface pH and measured bulk pH, as well as the difference between predicted surface $S(\text{FeCO}_3)$ and bulk $S(\text{FeCO}_3)$. The reason to compare these two sets of parameters is because $S(\text{FeCO}_3)$ is a function of pH, and the precipitation rate is linearly dependent on $S(\text{FeCO}_3)$ as follows:

$$PR_{\text{FeCO}_3} = k_{r,\text{FeCO}_3} e^{-\frac{\Delta G_{\text{FeCO}_3}}{RT}} K_{sp,\text{FeCO}_3} (S_{\text{FeCO}_3} - 1) \quad (25)$$

where the k_{r,FeCO_3} is a kinetic constant and the ΔG_{FeCO_3} is the activation energy for FeCO_3 precipitation.

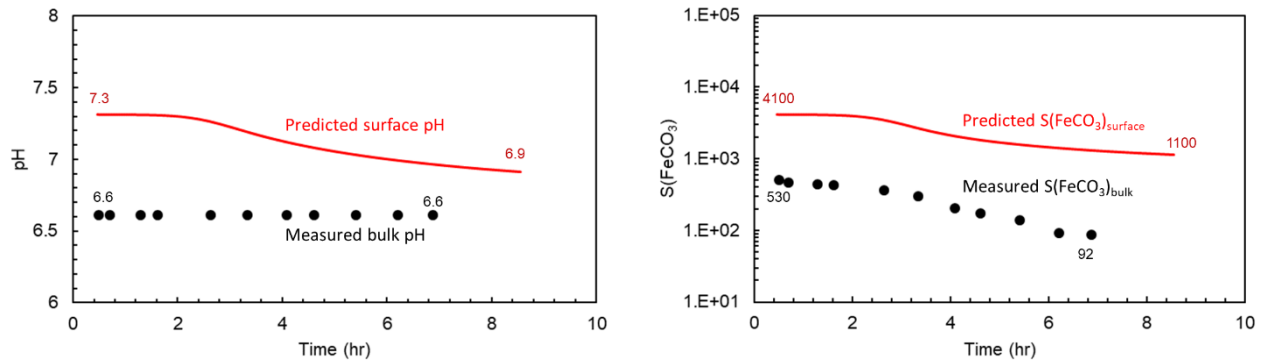


Figure 10. Comparison between predicted surface pH vs. bulk pH (left) and predicted surface S(FeCO₃) vs. bulk S(FeCO₃) (right) during FeCO₃ precipitation on an actively corroding surface, 70°C, pH 6.6, P_{total} = 1 atm, 1wt% NaCl, initial bulk S(FeCO₃) = 600

Figure 10 (left) shows the comparison of pH from the bulk and surface when using an actively corroding specimen surface. The measured pH in the bulk solution remained at pH6.6 and the predicted surface pH is almost a full pH unit higher as explained previously in Figure 9. The predicted surface pH is initially 0.7 pH unit higher, which is due to a rapid release of Fe²⁺ ions and the consumption of H⁺ in the early stage of corrosion. The pH difference between surface and bulk started to decrease after about two hours, and the final predicted surface pH was only 0.3 pH units higher than in the bulk solution. The decrease in surface pH was a result of FeCO₃ precipitation since CO_{3, aq}²⁻ on the surface was consumed to form FeCO₃ as indicated in Reaction (26)



Even though there was an ample amount of CO₃²⁻ in the bulk, the surface concentration of CO₃²⁻ was strictly limited by diffusion and convection. The quick decrease in CO₃²⁻ promoted the dissociation of H₂CO₃ and HCO₃⁻ to produce more CO₃²⁻ and H⁺, another product during this two-step H₂CO₃ dissociation process, as showed in Reaction (12) and (13). This decrease in pH during FeCO₃ precipitation also occurred during FeS precipitation.

Figure 10 (right) shows the calculated S(FeCO₃) from measured bulk pH and predicted surface pH when using an actively corroding sample surface. The measured initial S(FeCO₃) was 530. This started to decrease significantly after two hours and became stable after about six hours during the experiment. The predicted surface S(FeCO₃) exhibited the exact same trend, meaning that the bulk speciation somewhat affected the surface speciation. The ratio between bulk and surface saturation values was about 8 to 10.

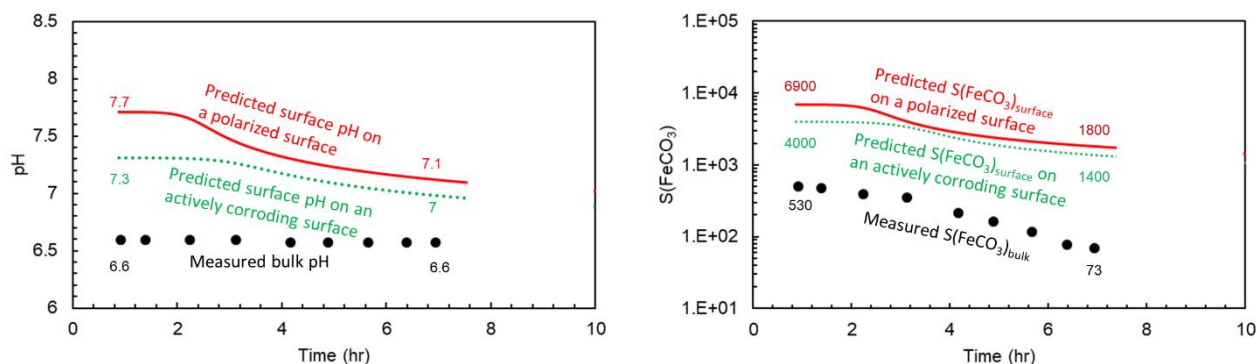


Figure 11. Comparison between predicted surface pH vs. bulk pH (left) and predicted surface $S(\text{FeCO}_3)$ vs. bulk $S(\text{FeCO}_3)$ (right) during FeCO_3 precipitation on a cathodically polarized surface, 70°C , pH 6.6, $P_{\text{total}} = 1 \text{ atm}$, 1wt% NaCl, initial bulk $S(\text{FeCO}_3) = 600$.

Measured bulk pH and predicted surface pH on a cathodically polarized specimen are compared in Figure 11 (left). Similar to the previous two cases, the bulk pH in this condition was also stable and the surface pH was constantly higher, even though it decreased after a few hours due to FeCO_3 precipitation. The prediction of surface pH on an actively corroding specimen is also included in this figure. It can be easily seen that despite the fact that the surface pH from both predictions is higher than the bulk value, the cathodic polarization increases surface pH further, as protons are consumed faster due to polarization.

$S(\text{FeCO}_3)$ calculated based on the pH values on a cathodically polarized specimen are presented in Figure 11 (right). By using a cathodically protected specimen, the predicted surface $S(\text{FeCO}_3)$ was about 15-25 times higher than the measured bulk $S(\text{FeCO}_3)$. This ratio was also higher than the predicted surface $S(\text{FeCO}_3)$ on an actively corroding specimen as shown in the figure. If compared with the last case for an actively corroding specimen where the predicted surface $S(\text{FeCO}_3)$ was only 8-10 times higher, the precipitation rate of FeCO_3 should be higher on a polarized specimen, which exactly agrees with the results discussed in Figure 1.

In FeS Formation Environment

Similar to the previous discussions in the FeCO_3 section, two sets of parameters are compared for FeS: the difference between the predicted surface pH and measured bulk pH, as well as the difference between the predicted surface $S(\text{FeS})$ and bulk $S(\text{FeS})$. Based on the results from Figure 2, the discrepancy between FeS precipitation rates measured on cathodically protected or free corroding surfaces was much more significant than for the same measurements with FeCO_3 precipitation. This implies that the speciation difference between the surface and bulk during FeS precipitation was greater when using different specimens.

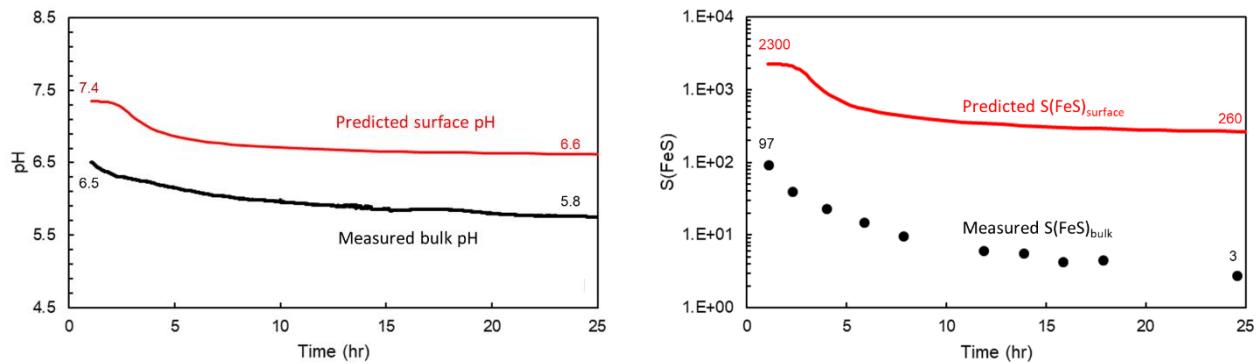


Figure 12. Comparison between predicted surface pH vs. measured bulk pH (left) and predicted surface S(FeS) vs. bulk S(FeS) (right) during FeS precipitation on an actively corroding surface, 70°C, initial pH 6.6, $P_{\text{total}} = 1 \text{ atm}$, $\text{pH}_2\text{S} = 100\text{ppm}$, 1wt% NaCl, initial bulk S(FeS) = 100.

Figure 12 (left) shows the comparison of measured bulk pH and predicted surface pH when using an actively corroding specimen surface. Unlike the same experiment in a CO_2 environment (Figure 10), the bulk solution pH also decreased during the process. This is because the low concentration of H_2S used in the experiment was not enough to compensate for the pH change caused by the FeS precipitation in the bulk solution, so that both bulk pH and surface pH had to change as simply defined using the electro-neutrality equation.

Figure 12 (right) shows the S(FeS) calculated based on measured bulk pH and predicted surface pH when using an actively corroding specimen surface. The predicted S(FeS) was about 20 times higher at the beginning stage of precipitation and this ratio kept rising. By the end of the experiment, the predicted S(FeS) was two orders of magnitude higher than the measured bulk S(FeS).

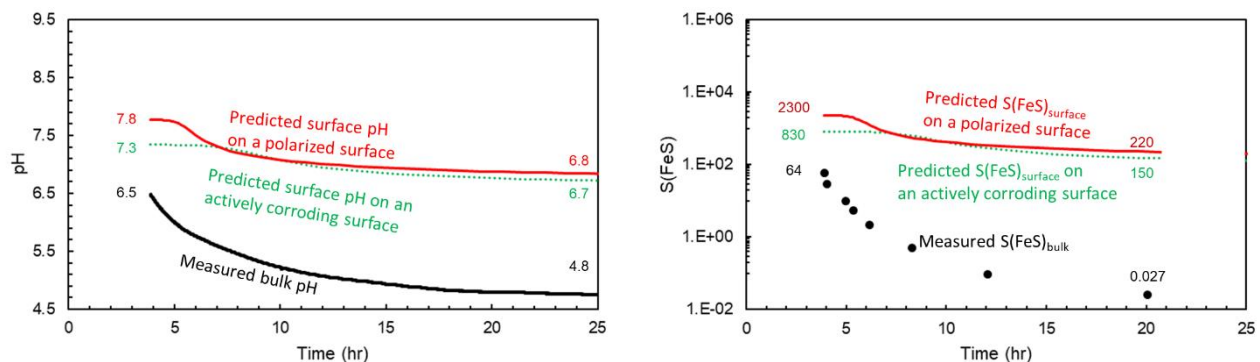


Figure 13. Comparison between predicted surface pH vs. measured bulk pH (left) and predicted surface S(FeS) and bulk S(FeS) (right) during FeS precipitation, 70°C, initial pH 6.6, $P_{\text{total}} = 1 \text{ atm}$, $\text{pH}_2\text{S} = 100\text{ppm}$, 1wt% NaCl, initial bulk S(FeS) = 80.

Measured bulk pH and predicted surface pH on a cathodically polarized specimen are compared in Figure 13 (left). Again, pH values for the bulk solution and at the surface both decreased with time, where the bulk pH decreased by almost two pH units. This is much higher than the previous experiment using an actively corroding specimen, where the pH change in bulk solution was less than one pH unit.

Clearly more FeS was precipitated when using a cathodically polarized surface and the pH had to change more to balance the electro-neutrality equation. Similar to the experiment explained in Figure 10 as related to FeCO₃, the surface pH on this polarized surface was also higher than the freely corroding surface, as shown in the same figure.

Calculated S(FeS) are presented in Figure 13 (right) for precipitation on a cathodically polarized surface. It is not surprising that the predicted S(FeS) on a polarized surface was higher than the one calculated for an actively corroding surface and the one measured in the bulk solution. The difference between measured bulk values and the predicted values using the cathodic polarized specimen surface was from 40 times to almost four orders of magnitude larger. Given the fact that the difference between S(FeS) for bulk and surface for the actively corroding case was less than two orders of magnitude as discussed in Figure 12, the predictions for the S(FeS) on a polarized surface verified the hypothesis that the speciation difference between a polarized and a freely corroding surface was greater during FeS precipitation, since the difference is only within a few factors for S(FeCO₃) in two different specimen conditions.

CONCLUSIONS

- A new *Polarization Model* was developed to predict surface speciation under cathodic polarization.
- The *Polarization Model* was confirmed to give reasonable predictions in conditions with and without the formation of a corrosion product layer.
- Based on the model predictions, surface speciation can be very different from bulk speciation with or without cathodic polarization.

ACKNOWLEDGEMENTS

The author would like to thank the following companies for their financial support:

Anadarko, Baker Hughes, BP, Chevron, CNOOC, ConocoPhillips, DNV GL, ExxonMobil, M-I SWACO (Schlumberger), Multi-Chem (Halliburton), Occidental Oil Company, PTT, Saudi Aramco, SINOPEC (China Petroleum), and Total.

REFERENCES

- 1 W. Sun and S. Netic, "Kinetics of corrosion layer formation: part 1—iron carbonate layers in carbon dioxide corrosion," *Corros. J.* 64,(2008): pp. 334-346.
- 2 Y. Zheng, "Electrochemical Mechanism and Model of H₂S Corrosion of Carbon Steel," Ph.D. Dissertation, Dept. Chem. Eng., Ohio Univ., Athens, OH, 2015.
- 3 K.-L. J. Lee, "A Mechanistic Modeling of CO₂ Corrosion of Mild Steel in the Presence of H₂S," Ph.D. Dissertation, Dept. Chem. Eng., Ohio Univ., Athens, OH, 2004.
- 4 Z. Ma, Y. Yang, B. Brown, S. Netic, and M. Singer, "Investigation of precipitation kinetics of FeCO₃ by EQCM," *Corros. Sci.* 141,(2018): pp. 195-202.

- 5 Z. Ma, B. Brown, S. Nescic, and M. Singer, "Investigation of FeS Precipitation Kinetics by EQCM," CORROISON/2019, paper no. 13425, (Nashville, Tennessee, 2019).
- 6 Z. Ma, B. Brown, S. Nescic, and M. Singer, "Precipitation Kinetics of FeCO₃ in Non-Ideal Solutions," CORROISON/2020, paper no. 14987, (2020).
- 7 W. Sun, "Kinetics of Iron Carbonate and Iron Sulfide Scale Formation in CO₂/H₂S Corrosion," Ph.D. Dissertation, Dept. Chem. Eng., Ohio Univ., Athen, OH, 2006.
- 8 Y. Zheng, J. Ning, B. Brown, and S. Nescic, "Advancement in predictive modeling of mild steel corrosion in CO₂- and H₂S- containing environments," *Corros. J.* 72,(2016): pp. 679-691.
- 9 M. Nordsveen, S. Nescic, R. Nyborg, and A. Stangeland, "A mechanistic model for carbon dioxide corrosion of mild steel in the presence of protective iron carbonate films part 1: Theory and verification," *Corros. J.* 59,(2003): pp. 433-456.
- 10 B. Brown, K.-L. J. Lee, and S. Nescic, "Corrosion in Multiphase Flow Containing Small Amounts of H₂S," CORROSION 2003, paper no. 03341, (Houston, Texas, 2004).
- 11 T. Tran, B. Brown, and S. Nescic, "Corrosion of Mild Steel in an Aqueous CO₂ Environment – Basic Electrochemical Mechanisms Revisited," CORROSION 2015, paper no. 5671, (Dallas, TX, 2015).
- 12 A. Kahyarian, B. Brown, and S. Nescic, "Mechanism of CO₂ Corrosion of Mild Steel: A New Narrative," CORROSION 2018, paper no. 11232, (Phoenix, Arizona, 2018).
- 13 A. Kahyarian and S. Nescic, "H₂S corrosion of mild steel: A quantitative analysis of the mechanism of the cathodic reaction," *Electrochim. Acta* 297,(2018): pp. 676-684.
- 14 S. Nescic and K. L. J. Lee, "A mechanistic model for carbon dioxide corrosion of mild steel in the presence of protective iron carbonate films—part 3: film growth model," *Corros. J.* 59,(2003): pp. 616-628.
- 15 Y. Zheng, J. Ning, B. Brown, and S. Nescic, "Electrochemical model of mild steel corrosion in a mixed H₂S/CO₂ aqueous environment in the absence of protective corrosion product layers," *Corros. J.* 7,(2015): pp. 316-325.
- 16 J. Han, B. Brown, D. Young, and S. Nescic, "Mesh-capped probe design for direct pH measurements at an actively corroding metal surface," *J. Appl. Electrochem.* 40,(2010): pp. 683-690.
- 17 R. Motte, R. Mingant, J. Kittel, F. Ropital, P. Combrade, S. Necib, *et al.*, "Near surface pH measurements in aqueous CO₂ corrosion," *Electrochim. Acta* 290,(2018): pp. 605-615.